Synthesis and characterization of Co-doped $BiFeO_3$

A THESIS SUBMITTED IN PARTIAL FULFILMENT OF THE REQUIREMENTS FOR THE DEGREE OF

Master of Science in Physics

By

Achyuta Kumar Biswal

Under the supervision of

Dr. Prakash N. Vishwakarma

DEPARTMENT OF PHYSICS

NATIONAL INSTITUTE OF TECHNOLOGY, ROURKELA

2008-2010

CERTIFICATE

THIS IS TO CERTIFY THAT THE THESIS ENTITLED "SYNTHESIS AND CHARACTERIZATIZATION OF CO-DOPED $BiFeO_3$" SUBMITTED BY MR. ACHYUTA KUMAR BISWAL IN PARTIAL FULFILMENT OF THE REQUIREMENTS FOR THE AWARD OF MASTER OF SCIENCE DEGREE IN PHYSICS AT NATIONAL INSTITUTE OF TECHNOLOGY, ROURKELA, IS AN AUTHENTIC WORK CARRIED OUT BY HIM UNDER MY SUPERVISION AND GUIDANCE.

TO THE BEST OF MY KNOWLEDGE, THE MATTER EMBODIED IN THE THESIS HAS NOT BEEN SUBMITTED TO ANY OTHER ORGANIZATION.

Date:

Prof. Prakash N. Vishwakarma

Dept. of Physics

National Institute of Technology

Rourkela – 769008

ACKNOWLEDGEMENTS

On the submission of my thesis "***Synthesis and characterization of Co - doped BiFeO3***", I would like to convey my gratitude & sincere thanks to my supervisor **Prof. Prakash N. Vishwakarma**, Department of Physics for his constant motivation and support during the course of my work in the last one year. I truly appreciate and value his esteemed guidance and encouragement from the beginning to the end of this thesis. I am indebted to him for having helped me shape the problem and providing insights towards the solution.

I am grateful to Dr Pawan Kuamr, Department of Physics for giving me the liberty to use all his instruments.

I am grateful to Dr B. Ganguly, HOD Physics for providing a very nice computer lab for the research work.

I am thankful to Dr S. K. Pratihar, Department of Ceramic Engineering for the thermal measurements.

I would like to thank Dr D. Pradhan, Department of Physics for use of some necessary chemicals and instruments.

I want to thank specially Miss Jashashree Ray PhD scholar department of Physics for helping me right from the beginning.

I want to thank Miss Mousumi, Mr Prakash, Mr Barun and Mr Naresh for their necessary help. I also like to thank all the teachers and all PhD, M Tech(R) scholar for their valuable suggestions.

I am grateful to the institute, National Institute of Technology Rourkela for having a very good laboratory facility.

Above all, I would like to thank all my friends whose direct and indirect support helped me completing my project in time. This thesis would have been impossible without their perpetual moral support.

Achyuta Kumar Biswal

Roll no: 408PH105

CONTENTS

Abstract

Multiferroic $BiFeO_3$ and the cobalt doped $BiFeO_3$ sample is prepared by sol – gel combustion technique using 2–methoxy ethanol and ethylene glycol as fuel. X-ray diffraction results confirm the formation of $BiFeO_3$ as major phase with small amount of impurity phases, which are subsequently removed by leaching the sample with dilute nitric acid. The Rietveld refinement of all compositions shows there is a gradual decrease in lattice parameter with increase in cobalt concentration. DSC and TG plots of the samples shows there is a structural phase change from R3c to P3mm at 829^0C and at higher temperatures appearance of impurity phases due to bismuth loss and liquid phases are seen. The SEM images of the sintered pellet show that the sample so prepared are having distribution of grain sizes which varies from 100nm - 1μm. The grains shrink to smaller size, when the sample is doped with cobalt. EDXS of sample shows that the elemental composition is free from any foreign elements contamination. Dielectric measurement is done for all the samples from 100Hz to 1MHz. The low frequency dielectric constant of undoped sample is 36 and increases to 202 for 10% cobalt doped sample.

CHAPTER 1: REVIEW & MOTIVATION

I. RECENT TRENDS OF RESEARCH ON OXIDES:

Since very beginning metal oxides have been the most focussed study from application as well as fundamental physics point of view. Their properties are strongly related to their structure, and variety of interesting physics has been witnessed on varying the external stimuli such as temperature and pressure. These properties have not only opened the door for various applications but also a better understanding of the physics involved. Some of the interesting properties include superconductivity, ferroelectricity, magnetism and multiferroicity.

1.1 Superconducting Oxides:

Until Bednorz & Muller reported superconductivity (1986) at ~23K in an oxide based compound, the superconducting phenomenon was considered only as low (Helium) temperature business and hence limited applications. Soon other oxide based superconductors were discovered whose superconducting transition temperature was much above that predicted by BCS theory for conventional superconductors, hence termed high temperature superconductor (HTS). Some of the HTS are listed in the chronological order of transition temperature in table-1 [1].

Table-1

Material	T_c (K)
**RE $Ba_2Cu_3O_7$ (REBCO)	90
$Bi_2Sr_2Ca_{1-x}Cu_nO_{2n+4}$(BSSCO)	122
$TiBa_2Ca_{n-1}Cu_nO_{2n+4}$(TBSSCO)	127
$TiBa_2Ca_{n-1}Cu_nO_{2n+3}$(TBSSCO)	122
$HgBa_2Ca_{n-1}Cu_nO_{2n+2}$	128

**RE: Rare-earth elements including Yttrium(Y) and Lanthanum (La).

1.2 Ferroelectic Oxides:

Ceramic oxides with non-centrosymmentric perovskite structure generally show ferroelectricity. These oxides are used in bulk and thin film form for various applications. The ferroelectric properties of these oxides make them for use as non-volatile memory. The piezoelectric property of these materials enhances their use in actuators and ultrasound imaging. The high dielectric constant of these materials facilitates there use in capacitors and memory devices. The ferroelectric, piezoelectric and dielectric properties of the material are enhanced by doping the material with suitable dopants [2]. Now the current trend is to synthesize the ferroelectric oxides which give above properties at room temperature, for their applications. These oxides include $BaTiO_3$, $CaTiO_3$, $PbTiO_3$ and $SrTiO_3$ along with suitable dopants. Due to toxicity and high volatility of Lead (Pb), now a day there is awareness for synthesizing the lead free ceramic oxides for ferroelectric application. The different ferrolelectic oxides with their dielectric constant values are given in table – 2.

Table - 2

Material	Dielectric constant
$SrTiO_3$	310
$Ba_{1-x}Sr_xTiO_3$	500
$BaTiO_3$	1250–10,000 (20–120 °C)
$CaTiO_3$	300
$(La,Nb,Zr,Ti)PbO_3$	500–6000

1.3 Magnetic Oxides:

Magnetic materials have become an integral part of our day-to-day life, owing to their various applications in different areas. Generally magnetic materials can be classified in soft and hard form, from the view point of magnetic property. The soft magnets are the magnets having low coercivity in the hysteresis loop and vice – versa. The magnetic oxides are generally soft magnets. Due to low coercivity they are used into an alternating magnetic field [2]. They show excellent magnetic property in high frequency as compared with metal magnetic materials. They show high electrical resistivity and smaller eddy current loss. These soft magnetic oxides generally include ferrites, mangenites and cobaltites. Generally soft ferrites exist in two types of structures, i.e., spinel type and garnate type. They show the properties like high curie temperature, high permeability and high stability. Transition metals like iron (Fe), cobalt (Co) manganese (Mn) and nickel (Ni) combining with oxygen and other materials results various oxides [2]. Various magnetic oxides with their magnetic flux density and Curie temperature values are listed in the table -3.

Table -3

Chemical formula	Magnetic flux density (Tesla) at room temperature	Ferromagnetic Curie temperature(T_c) in K
$MnFe_2O_4$	400	570
$CoFe_2O_4$	480	790
$NiFe_2O_4$	270	860
Y_3FeO_{12}	135	550
$Ba_3Co_2Fe_{24}O_{41}$	270	683

1.4 Multiferroic Oxides:

These oxides have the unique properties of both ferromagnetism and ferroelectricity in a single crystal. This opens broader applications in transducers, magnetic field sensors and information storage industry. These include $BiFeO_3$, $BiMnO_3$, $TbMnO_3$, $TbMn_2O_5$, $YMnO_3$,

$LuFeO_4$ and $Ni_3B_7O_{13}I$. Among these oxides $BiFeO_3$ (**BFO**) is the only material which gives ferroelectricity and antiferromagnetism at room temperature.

Due to coexistence of both ferromagnetism and ferroelectricity in the same material, it is expected to exhibit ferromagnetic & ferroelectric properties or a coupling of these two properties in a single material. This increases the current range of application and moreover interesting physics may be observed. Presently lot of research work is carried out on this particular field in different forms like bulk, powder, thin film and nanostructure.

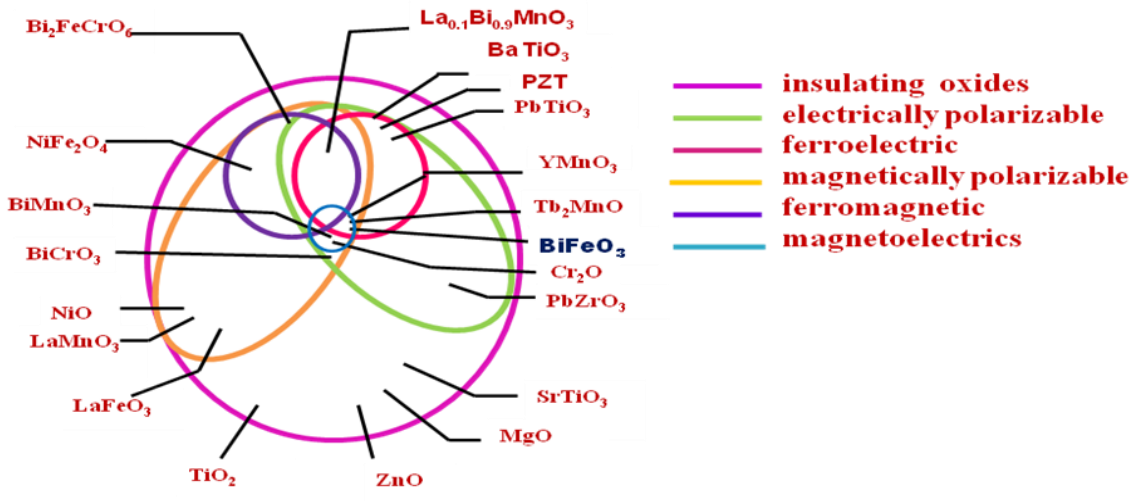

Figure 1(a). Shows the various oxides categorized by their behaviour in electric and magnetic field.

II. MULTIFERROICS AND MAGNETOELECTRICITY:

A single phase multiferroic material is one that possesses two of the three 'ferroic' properties i.e ferroelectricity, ferromagnetism and ferroelasticity. Generally current trend is to exclude the requirement for ferroelastic property. Magnetoelectric coupling describes the coupling between magnetic and electric order parameters. The classification of various ferroic and magnetic and electic order parameter coupling is given in the next page [3].

The relationship between multiferroic and magnetoelectric is well reflected by figure-1. The figure describes that magnetically (electrically) polarisable materials form the superset of ferromagnetic (ferroelectric) materials. The intersection between them represents the

multiferroic materials. The confluence of the three regions is the current high level of research.

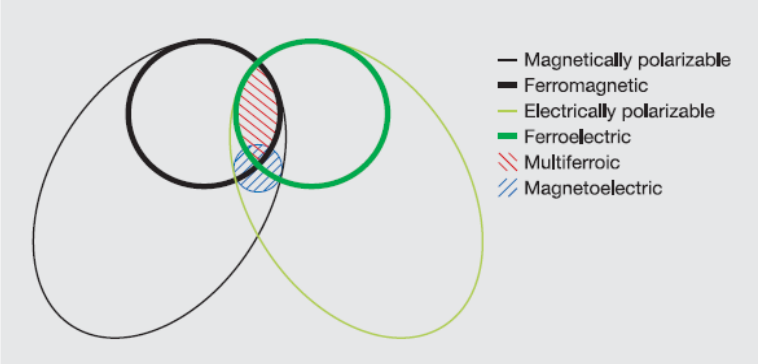

Figure 1(b). shows the intersection of two sets named magnetically and electrically polarizable material with subsets of ferromagnetic, ferroelectric, and intersection called multiferroic and magneto electric[3].

III. Classification of Ferroics [3]:

Ferroelectric materials possess a spontaneous polarization that is stable and can be switched hysteretically by an applied electric field;

Antiferroelectric materials possess ordered dipole moments that cancel each other completely within each crystallographic unit cell.

Ferromagnetic materials possess a spontaneous magnetization that is stable and can be switched hysteretically by an applied magnetic field;

Antiferromagnetic materials possess ordered magnetic moments that cancel each other completely within each magnetic unit cell.

Ferroelastic materials display a spontaneous deformation that is stable and can be switched hysteretically by an applied stress.

Ferrotoroidic materials possess a stable and spontaneous order parameter that is taken to be the curl of a magnetization or polarization. By analogy with the above examples, it is anticipated that this order parameter may be switchable.

Ferrimagnetic materials differ from antiferromagnets because the magnetic moment cancellation is incomplete in such a way that there is a net magnetization that can be switched by an applied magnetic field.

Order parameter coupling:

Magnetoelectric coupling describes the influence of a magnetic (electric) field on the polarization (magnetization) of a material.

Piezoelectricity describes a change in strain as a linear function of applied electric field, or a change in polarization as a linear function of applied stress.

Piezomagnetism describes a change in strain as a linear function of applied magnetic field, or a change in magnetization as a linear function of applied stress.

Electrostriction describes a change in strain as a quadratic function of applied electric field.

Magnetostriction describes a change in strain as a quadratic function of applied magnetic field.

IV. MORE ON $BiFeO_3$:

- $BiFeO_3$ is the only prototype among all other multiferroic oxides which shows both ferromagnetism and ferroelectricity in a single crystal above room temperature. It has ferroelectric Curie temperature T_c = 1143K and antiferromagnetic Neel temperature T_N = 643K [3].

- The ions responsible for the production of ferroelectricity and magnetism are Bi^{3+} and Fe^{+3} ions. Ferroelectricity is produced due to Bi^{3+} and antiferromagnetism is due to Fe^{+3} ions [3].

CRYSTAL STRUCTURE:

- It is having rhombohedrally distorted perovskite structure with R3c space group at room temperature.

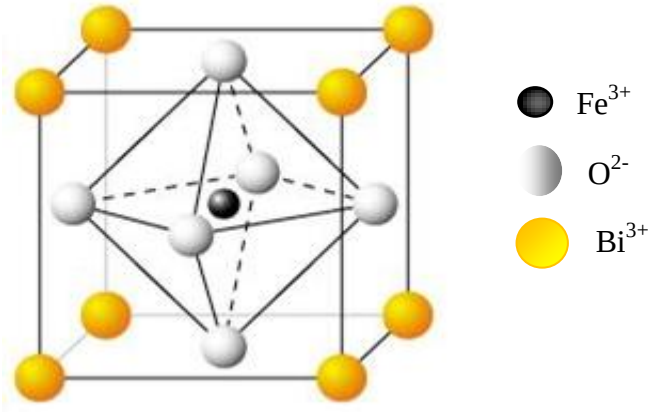

Fig 2. $BiFeO_3$ in Perovskite structure

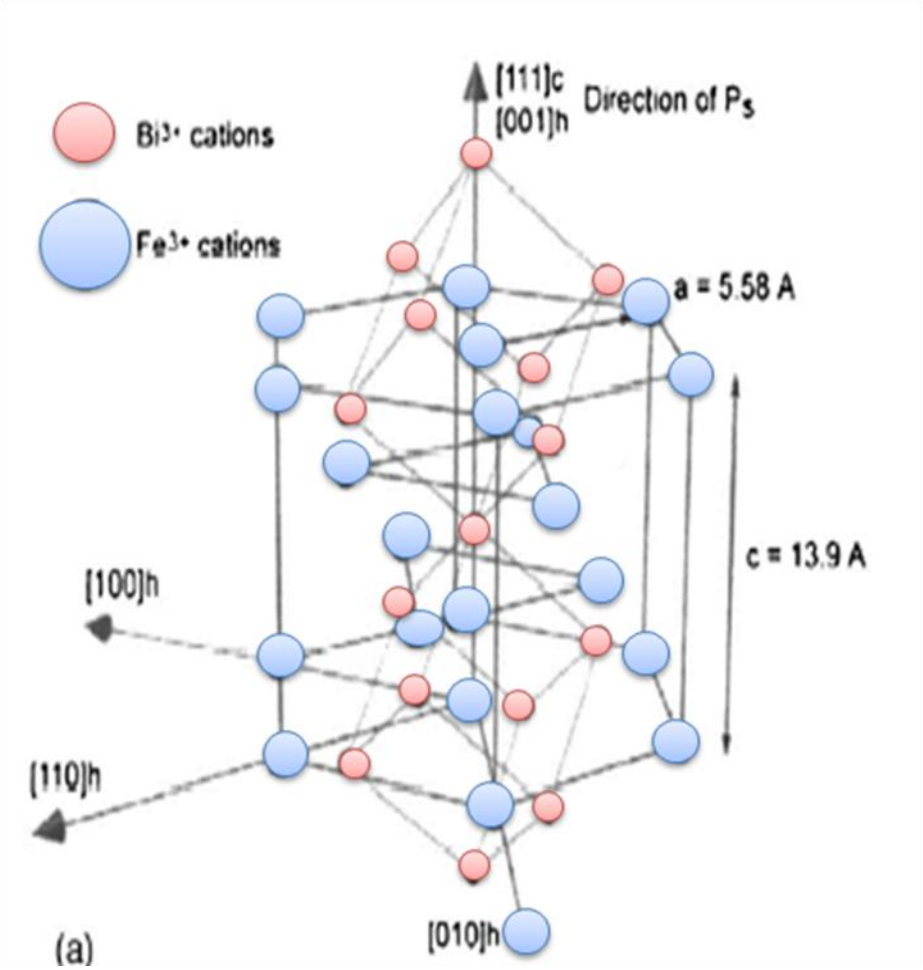

Figure 3. Arrangement of individual blocks in crystallographic lattice and the [111] polarized direction.

- Bi^{3+} ion occupy the corner position, Fe^{3+} in the body centred position, and O^{2-} in all face centred position. The lattice parameters are a = 5.587 A^0, b = 5.587 A^0 and c = 13.867 A^0 with $\alpha = \beta = 90^0$ and $\gamma = 120^0$. The hexagonal unit cell contains 6 formulas.

- Generally ferroelectricity is produced by vacant d^0 orbital and ferromagnetism is observed due to partially filled d^n orbital. In $BiFeO_3$, ferroelectricity is produced due to stereo chemical activity of Bi^{3+} ion and ferromagnetism is due to Fe^{+3} ions [3].

Production of ferroelectricty:

$Bi^{3+}$and Fe^{3+} cations displaced along the [1 1 1] threefold polar axis and off centred with respect to the barycentre of the oxygen octahedron, which in turn gives rise to ferroelectricity[4].

Production of ferromagnetism:

It is produced due to rotations of adjacent oxygen FeO_6 octahedral around the [1 1 1] pseudo cubic direction (figure-3). The Fe^{3+} magnetic moments are ordered in a manner that of a ***G-type antiferromagnetic ordering*** [4].

- **G-Type antiferromagnetic ordering**: Nearest neighbour Fe^{+3} magnetic moments are aligned antiparallels to each other in all three Cartesian directions.

APPLICATIONS:

- Due to multiferroic nature of $BiFeO_3$ it has broader applications in the field of transducers, magnetic field sensors and information storage industry [3].

- Due to its magnetoelectric coupling it has the advantage that data can be written electrically and read magnetically. It exploits the best aspects of ferroelectric random access memory (FeRAM) and magnetic data storage. Multiferroism leads to fast, low-power consumption, multifunctional memory devices exploiting the best attributes of conventional ferroelectric and magnetic random-access memories [3].

- Recently, ferroelectric random access memories (FeRAMs) have achieved fast access speeds (5 ns), high densities (64 Mb) [3]

V. LITERATURE SURVEY:

1. Jiang *et al.*, J Electroceramics.21, 690 (2008):

- ✓ The $BiFeO_3$ ceramic sample shows low dielectric constant and low loss tangent between 100 Hz and 10 MHz. pH value has an effect on the purity of $BiFeO_3$.
- ✓ The sample via conventional sintering process has higher conductivity and cannot be polarized but has a low loss tangent.
- ✓ $BiFeO_3$ from spark plasma sintering has $\varepsilon = 45$ and loss of 0.1-1% at $T = 600^0C$ and ε increases to 80-100 and the loss tangent up to 1-10% for $T = 700^0C$.

2. Lebeugle *et al.*, Physical Review B.76, 024116 (2007):

- ✓ Highly pure single crystal of $BiFeO_3$ can be grown by flux method.
- ✓ Ferroelectric hysteresis loop is observed at room temperature.
- ✓ A way to obtain higher dielectric constant and lower loss factor is to make solid solution of $BiFeO_3$ with another ABO_3 that is BFO-$Pb(Ti,Zr)O_3$.
- ✓ In epitaxial thin film polarization increases to tenfold due to structural change.

3. Donna C. Arnold *et al.*, Physical Review Letters.102, 027602 (2009):

- ✓ $BiFeO_3$ undergoes a first order ferroelectric to paraelectric transition at T_C (820–830^0C) from a phase of R3c symmetry to an orthorhombic phase with Pbnm space group.
- ✓ The nature of the transition is markedly different to the rhombohedral to orthorhombic transition in ferroelectric $BaTiO_3$, and to the rhombohedral-orthorhombic (ferroelectric to antiferroelectric) transition in $NaNbO_3$.

4. Haumont *et al.*, Physical Review B.79, 184110 (2009):

- ✓ Pressure instabilities in the multiferroic $BiFeO_3$, it is revealed that two structural phase transitions around 3.5 and 10 GPa by using diffraction and far-infrared spectroscopy at a synchrotron source.
- ✓ The intermediate phase crystallizes in a monoclinic space group, with octahedral tilts and small cation displacements. When the pressure is increased further the cation displacements and thus the polar character of $BiFeO_3$ is suppressed above 10 GPa.

5. Kornev *et al.*, Physical Review Letters.99, 227602 (2007):

- ✓ An effective Hamiltonian scheme is developed to study finite-temperature properties of multiferroic $BiFeO_3$. This approach reproduces very well (i) the symmetry of the ground state, (ii) the Neel and Curie temperatures, and (iii) the intrinsic magnetoelectric coefficients.
- ✓ This scheme also predicts
    - An overlooked phase above T_c = 1100 K
    - Improper like dielectric features above T_c.
    - The ferroelectric transition is of first order with no group-subgroup relation between the paraelectric and polar phases.

6. Cheng *et al.*, Physical Review B.77, 092101 (2008):

- ✓ There is significant improvement of the ferroelectric properties of $BiFeO_3$ thin film through control of electrical leakage by Nb doping.
- ✓ A very large remnant electrical polarization value of 80 μC/cm2 was observed in Bi0.8La0.2Nb0.01Fe0.99O3 thin film on Pt/Ti/SiO2 / Si substrate.
- ✓ The doping effect of Nb in reducing the movable charge density due to oxygen vacancies in BiFeO3 was confirmed by the dielectric measurements.
- ✓ A very small loss was observed in the Nb and La co-doped $BiFeO_3$ thin film. As well as the improvement in the ferroelectric properties, the magnetic moment was also enhanced due to the doping of La.

7. Zhu *et al.*, Physical Review B.78, 014401 (2008):

- ✓ A series of multiferroic (1-x) $BiFeO_3$ - x$PbTiO_3$ solid solution ceramics were prepared by solid-state reactions.
- ✓ Structural characterization by x-ray diffraction reveals the existence of a morphotropic phase boundary (MPB) region in this system in which a tetragonal, a rhombohedral, and an orthorhombic phase exist simultaneously.
- ✓ The temperature variation of magnetic moment of the samples with MPB compositions, measured under zero-field cooling (ZFC) mode, shows three anomalies

arising from the antiferromagnetic orderings of the rhombohedral, tetragonal, and orthorhombic phases, respectively.

- ✓ The significant difference in antiferromagnetic ordering temperatures of the rhombohedral and tetragonal phases is attributed to the different structural effects on the magnetic interactions between the rhombohedral and the tetragonal phases, and the effect of the magnetic dilution on the magnetic ordering strength.
- ✓ The magnetic phase diagram of the $(1-x)$ $BiFeO3-xPbTiO_3$ solid solution system was established.

8. Lee *et al.*, Physical Review B.78, 100101 (2008):

- ✓ Studied on polarized neutron-scattering and piezoresponse force microscopy studies of millimetre-sized single crystals of multiferroic $BiFeO_3$.
- ✓ The crystals, grown below the Curie temperature, consist of a single ferroelectric domain. It has two unique electric polarization directions.

9. Cazayous *et al.*, Physical Review Letters.101, 037601 (2008):

- ✓ The magnetic spectra of $BiFeO_3$ were studied by means of low-energy inelastic light scattering. It is revealed that the existence of two species of magnons corresponding to spin wave excita tions in and out of the cycloidal plane.

CHAPTER 2: EXPERIMENTAL

Synthesis of the sample in single phase is the most important part of the research work. Different methods have been adopted for preparing the BFO in bulk, thin film and nano form. Some of the methods adopted for the synthesis of single phase BFO are summarized below.

1. SYNTHESIS LITERATURE SURVEY:

a. Carvalo *et al.*, Material Letters.62, 3984 (2008):

Sample is prepared by Sol gel combustion method with starting materials Bi_2O_3 (99.9%) and Fe_2O_3 (99.95%) dissolved in dilute nitric acid. Urea was used as fuel in molar ratio [urea] / {[Bi]+[Fe]} of 3. After ignition, brown powder was obtained. The powder was pressed into discs and then treated 500^0C and atmosphere.

b. Lebegule *et al.*, Physical Review B.76, 024116 (2007):

Stoichiometric Bi_2O_3 : Fe_2O_3 mixture is ground finely and sintered in air for 15hr at 800^0C using an alumina crucible. The crucible can only be used for one or two experiments. The analysis shows no traces $Bi_2Fe_4O_9$ but a small amount of $Bi_{25}FeO_{39}$. The parasitic phase can be removed by leaching with 10 % HNO_3.

c. Hardy *et al.*, Journal of European Ceramic Society.29, 3007 (2009):

Starting products for synthesis are Bi(III) citrate ($BiC_6H_5O_7$), Fe (III) citrate hydrate ($FeC_6H_5O_7.H_2O$), Fe(III) nitrate non hydrate ($Fe(NO_3)_3.9H_2O$) and citric acid. The concentration of metal ions to citric acid is equal to 1:1. 10 % Bi excess is added to compensate for eventual bismuth loss during thermal treatment.

d. Xue *et al.*, Materials Research Bulletin.43, 3368 (2008):

BFO powder was synthesized by a solution evaporation process. 0.01 mole of $Bi(NO_3)_3.5H_2O$ and 0.01 mol $Fe(NO_3)_3.9H_2O$ were initially dissolved in the dilute nitric acid to form a transparent solution. EDTA in 1:1 mole ratio with respect to the metal nitrates was added to the above solution. The solution is then heated at 130 ^{0}C under constant stirring in oil bath until all liquids get evaporated out from the solution. The powder was then collected

and sintered for 350s in air at different temperatures (300 – 600 ^{0}C) using rapid thermal processor with heating rate up to 80 ^{0}C/s to get $BiFeO_3$ nanoparticles.

e. Lee *et al.*, Applied surface science.254, 1493 (2007):

Co-substituted $BiFeO_3$ thin films are deposited on the Pt substrate by CSD method. $Bi(No_3)_3.5H_2O$,$Fe(NO_3)_3.9H_2O$ $Nd(No_3)_3.6H_2O$,$Sm(No_3)_3.6H_2O$ and $Cr(No_3)_3.9H_2O$ were used as starting materials and a mixture of 2-methoxy ethanol and ethylene glycol are mixed at room temperature for 30 minutes to make a homogenous solution. Acetic acid as a catalyst was added to the co-solvent and stirred for 30 minutes and the above salts are added one after another to the co-solvent with continuous stirring after 30 minutes to each. The concentration of precursor solution was adjusted to approximately 0.2 M .The Pt substrate is spin coated with the prepared precursor.

f. Jiang *et al.*, J Electroceramicics.21, 690 (2008):

The powders of BiFeO3 were prepared with the Pechini method. $Fe(NO_3)_3.9H_20$ and citric acid were taken in suitable stoichiometry and dissolved in required amount of distilled water. The solution was stirred and heated at 70 ^{0}C for 3 h to form a sol. Aqueous ammonia was used to adjust the pH value. $Bi(NO_3)_3$ .5 H_2O was then slowly added to the Fe – sol in order to avoid the precipitation of bismuth salts. The sol was dried at 130 ^{0}C in an oven for 12 h to form gel. The gel was slowly heated to 700 ^{0}C and then kept for 1 h to obtain $BiFeO_3$. The best result was obtained for solution having pH = 1.

g. Higuchi *et al.*, Physical review B.78, 085106 (2008):

$BiFeO_3$ sample was prepared by solid-sate reaction using conventional milling and firing techniques. Bi_2O_3 and Fe_2O_3 powders corresponding to $BiFeO_3$ composition with). 75 mol % of excess Bi was weighed and thoroughly mixed using stabilised ZrO_2 balls in ethanol. The mixtures were dried, pressed and sintered at 750 ^{0}C for 2 h with heating rate of 10 ^{0}C/min. In this case polyvinyl alcohol was used as binder. The powder compacts were subsequently sintered at 900 – 1000 ^{0}C for 3 – 10 h at an increment of 10 ^{0}C /min.

II. INFERENCE:

From the above mentioned literatures it is observed that generally there are two methods of preparation for BFO powder: the solid state root and the liquid phase root. In solid state root; oxides of bismuth, iron are taken and are grinded to form BFO powder. But in liquid phase root; nitrates of bismuth and iron are taken and are mixed in the liquid medium to obtain the same. In liquid phase technique the constituents are mixed in the atomic level and then the lattice growth occurs. But in solid state the powder is obtained by crossing the different planes in the lattice. Another advantage of Liquid phase combustion synthesis is that the chances of impurity are lesser than the solid state synthesis. So the liquid phase combustion synthesis is chosen for the preparation of the sample.

III. SYNTHESIS:

The samples are prepared by sol – gel combustion route. The fuel chosen for the synthesis is mixture of 2 – methoxy ethanol and ethylene glycol. 25 ml of 2- methoxy ethanol is added with 25ml of ethylene glycol and stirred for 30 minutes. It is reported that, solvent with pH:1 results best prepared sample [6], so the mixture of fuels are added to acetic acid drop wise with continuous stirring till the pH meter reading showed pH:1. It was noted that 26.6 ml of acid is mixed with 50 ml of fuel mixture in order to obtain pH:1. This value is considered as standardization for other samples as well. After 30 minutes of continuous stirring of the fuel and acid mixture, the stoichiometric amount of $Bi(NO_3)_3$ .5 H_2O salt is added and stirred for another 30 minutes. Then $Fe(NO_3)_3.9H_20$ salt is added to the mixture. Now the colour of the solution changes from colourless to brick red then red and finally blackish red. After 1 hour of continuous stirring the solution is heated with stirring at a temperature of 70^0C. After 3 hours of heating and stirring the solution became transparent gel. Then after few minutes and in some elevated temperature yellow colour precipitation occurred. This precipitate is found to be hygroscopic when left for 10 hours. So the sample is then again heated at a temperature 115 ^{0}C, to vaporise all the water content from the sample. After some time the powder in the bottom of beaker turned black, gradually the whole powder become blackish. The black powder is also found to be hygroscopic. With further heating it is found that the powder burnt with glows, exactly similar to charcoal cavity experiment with evolution of white coloured gases. Now the xerogel powder obtained is not hygroscopic. The powder collected is then calcined for 2 hours at a temperature of 500 ^{0}C. The furnace heating rate is maintained as 4 ^{0} /

minute. After cooling, the sample is collected from the furnace and is grinded by agate - mortar. The grinded powder is now ready for necessary characterization. To obtain the Co – doped BFO, $Co(NO_3)_3.6H_2O$ is added after $Bi(NO_3)_3$ .5 H_2O then followed by $Fe(NO_3)_3.9H_20$. The x-ray data revealed parasitic phases along with the $BiFeO_3$ as major phase. The parasitic phases are removed by leaching the sample with dilute HNO_3. Leaching is done by adding the powder in 1 molar solution of 70 % pure HNO_3 with continuous stirring for 2 hours. The solution is then centrifuged and dried to obtain the pure sample.

The sample is then pressed into pellet by dry pressing method and is then sintered at a temperature of 700 ^{0}C, for electrical characterization.

The exact procedure for the preparation of the sample is depicted by the flow chart below.

IV. FLOW CHART:

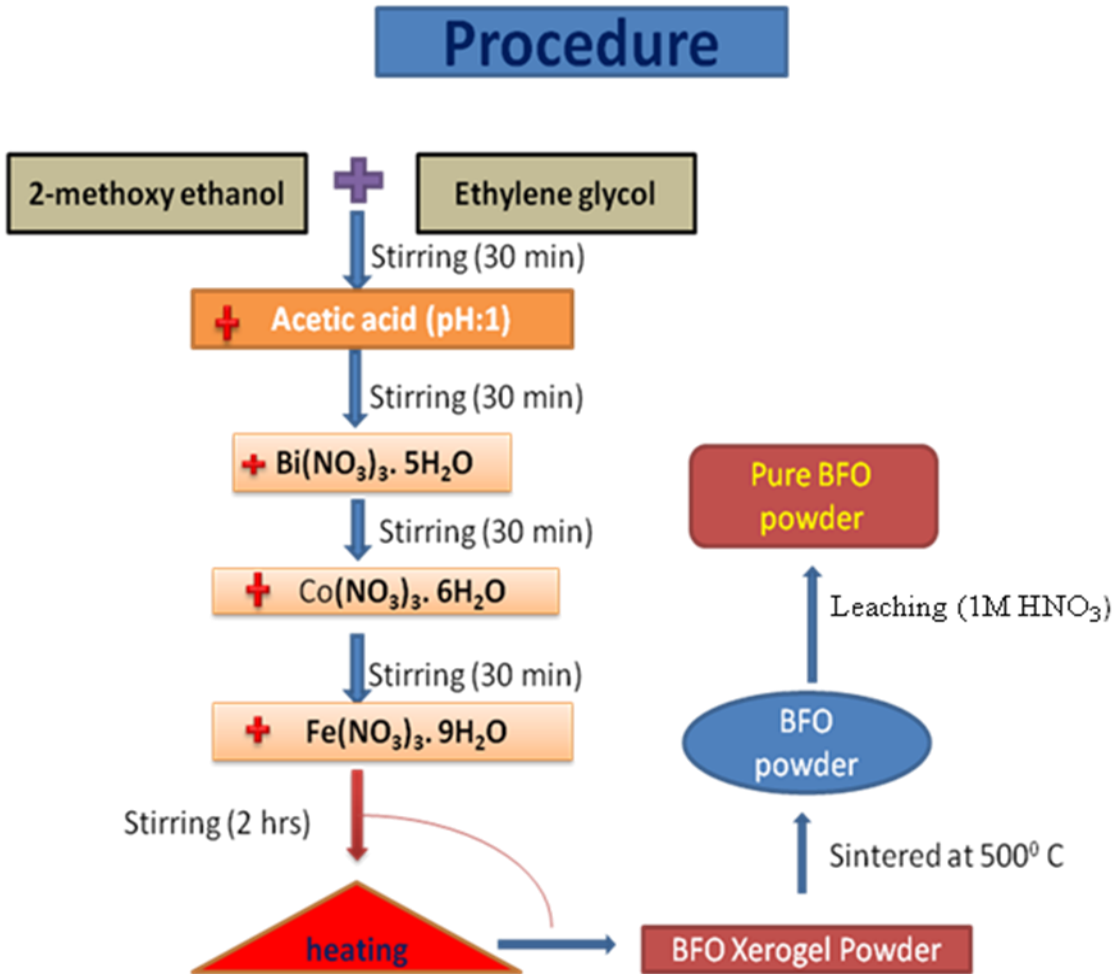

CHAPTER 3: RESULT & DISCUSSIONS

I. XRD Analysis:

Phase analysis was studied using the room temperature powder X-ray diffraction (Model: PW 1830 diffractometer, Phillips, Netherland) with filtered 0.154 nm Cu Kα radiation. Samples are scanned in a continuous mode from 20° – 80° with a scanning rate of 3^0/minute. The samples so prepared are calcined at various temperatures to optimise. XRD patterns of $BiFeO_3$ (BFO) ceramic calcined at 500^0C and 700^0C are shown in the figure 4(a). The prominent peaks in xrd plot are indexed to various hkl planes of BFO, indicating formation of BFO. Besides these prominent peaks, some other peaks of low intensity are also observed, which do not belong to BFO. The sample calcined at 700^0C is having many extra peaks other than BFO whereas that prepared at 500^0C is less impurity peaks. The literature survey of BFO synthesis relates these impurity peaks to be that of $Bi_2Fe_4O_9$ and $Bi_{25}FeO_{39}$. The appearance of these extra phases at 700^0C could be due to large bismuth loss at higher temperature. Powders calcined at 500^0C is having less impurity phase of $Bi_{25}FeO_{39}$ and $Bi_2Fe_4O_9$, as is evident from the lesser peak height than 700^0C one. Hence the calcination temperature is restricted to 500^0C for all the samples.

Figure 4(b) shows the x-ray diffraction plots of BFO, 5 % Co-doped BFO (CBFO5) and 10% Co-doped BFO (CBFO10). These results indicates that on cobalt doping up to 10 atomic % at Fe site, the rhombohedral structure of BFO does not change appreciably, except increase in $Bi_{25}FeO_{39}$ and $Bi_2Fe_4O_9$ impurity phases at 33^0 and 28^0. The 10% Co – doped BFO sample shows other impurities besides the above two phases. Presently the phases responsible for these peaks are not known but these phases can be are substantially removed by leaching the sample in dilute HNO_3 acid. The x-ray diffraction plots of leached samples are shown in figure 4(c), which shows that all the parasitic phases are removed. However, for 10% Co doped sample, one extra peak at 35^o is still present, and couldn't be removed. At present the origin of this peak is not known. The intensity of impurity peaks increases with increase in doping concentration, indicating increasing concentration of impurity phases.

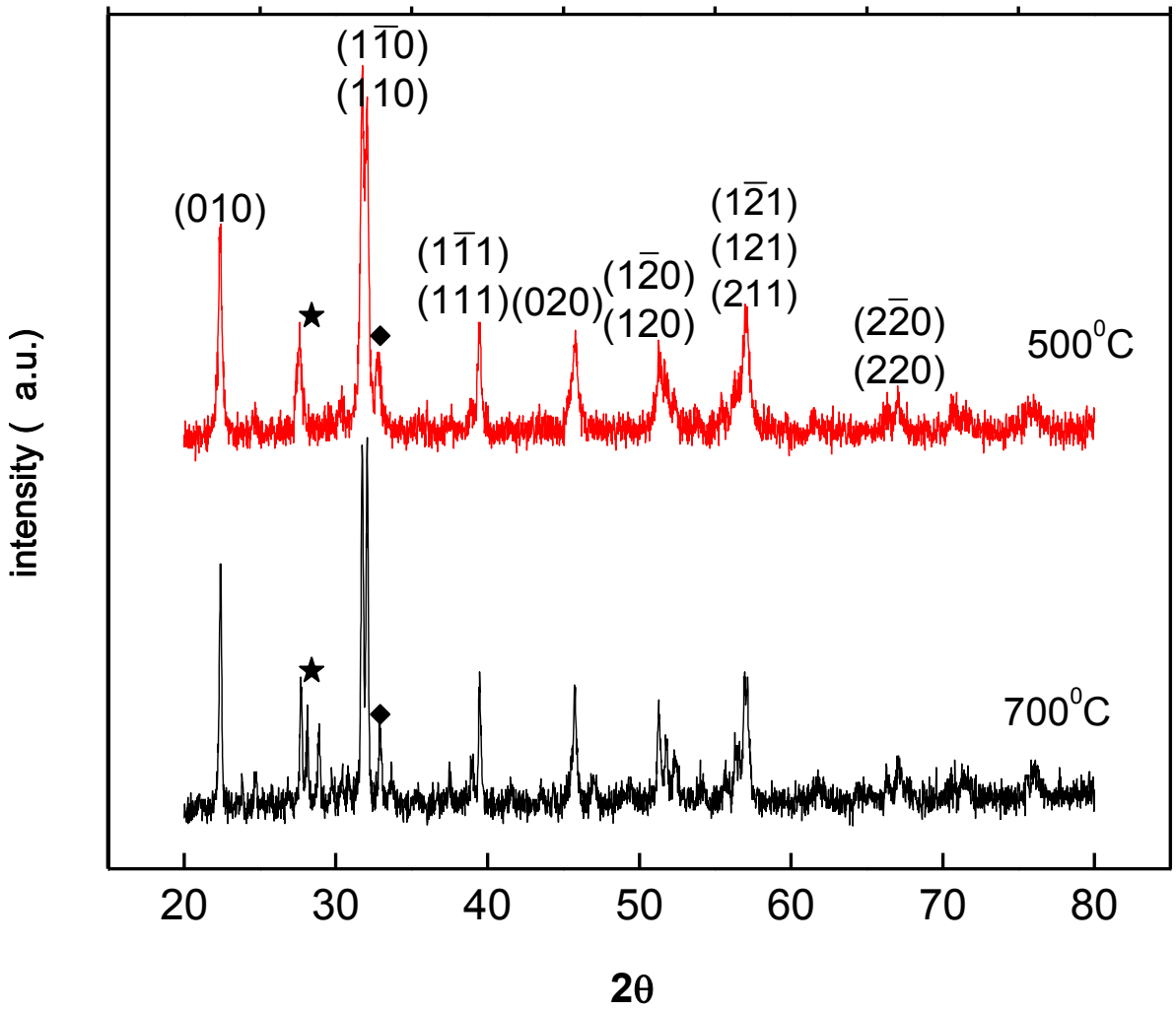

Figure 4(a). XRD plots of BFO calcined at 500^{0}C and 700^{0}C with impurity peaks at 28^0 and 33^0

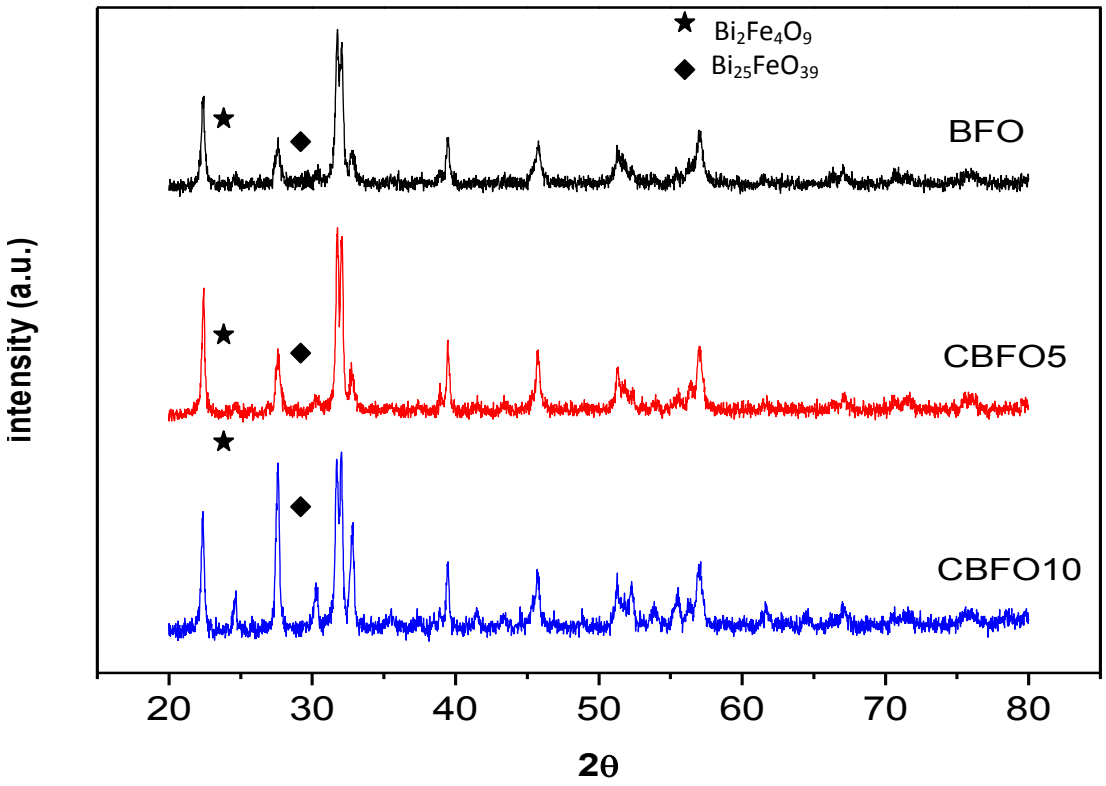

Figure 4(b). XRD plots of BFO, CBFO & CBFO10 (without leaching)

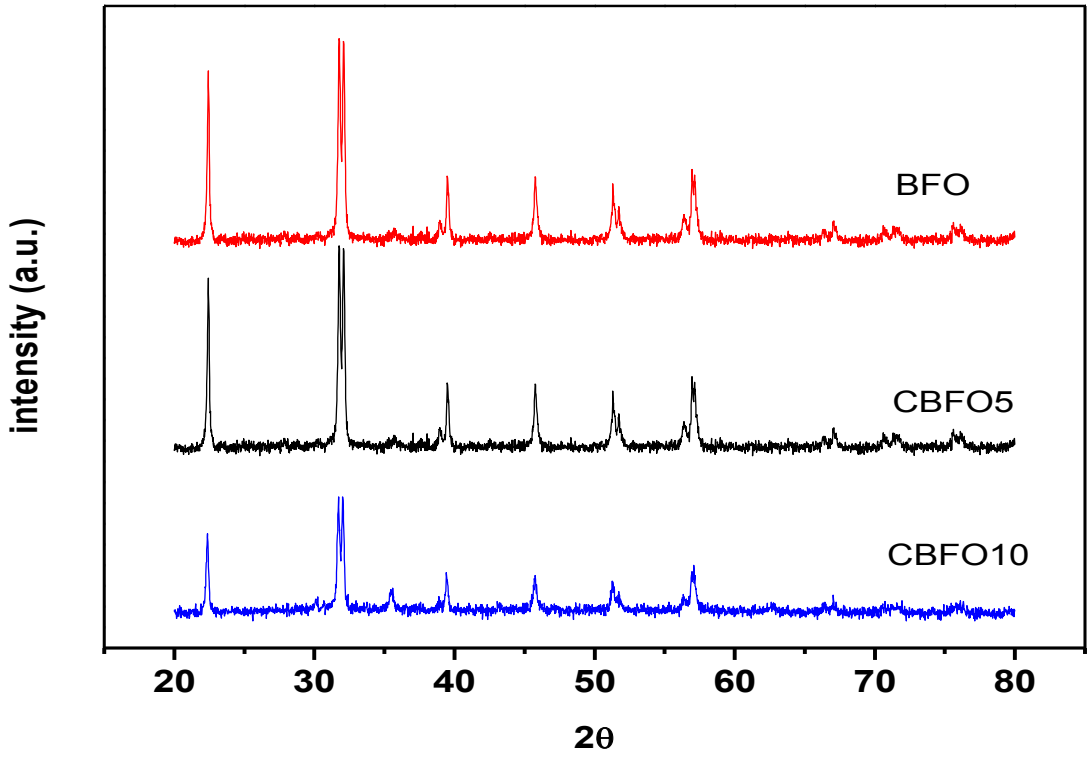

Figure 4(c). XRD plots after leaching with dilute HNO_3 acid. No impurity phases are seen

Rietveld refinement of X-ray results:

The x-ray diffraction data so obtained were further analysed by Reitveld refinement method using freely available software "FULPROF". The Rietveld refinement of all the three samples is carried out by considering the samples have rhombhedrally distorted perovskite structure with R3c space group [4]. The best fittings obtained for BFO, CBFO5 and CBFO10 are shown in figure 5(a), 5(b) & 5(c). The refined lattice parameters so obtained for all compositions are listed in the table-4. The integer in the bracket next to the lattice parameters are the corresponding error values. From these values of 'a', 'b' & 'c' it is revealed that the lattice parameters are decreasing with increase in cobalt concentration. Though the decrease in case of 'a' & 'b' is not prominent, but in 'c' it is clearly seen. So we can confirm here that for increase in Co – concentration there is a gradual shrinkage in unit cell volume [7]. This may be due to smaller ionic radius of Co^{3+} (74pm) ions than Fe^{3+} (78pm) [8]. This confirms that the Cobalt is successfully doped in the BFO lattice. The lattice parameter "c" observed for different concentration of cobalt is plotted in Figure 5 (d).

Table - 4

Sample name	Lattice parameter
BFO	a = b = 5.5773(2) c = 13.8721(9) α = β = 90, γ =120
CBFO5	a = b = 5.5735(8) c = 13.850(2) α = β = 90, γ =120
CBFO10	a = b = 5.5728(8) c = 13.849(2) α = β = 90, γ =120

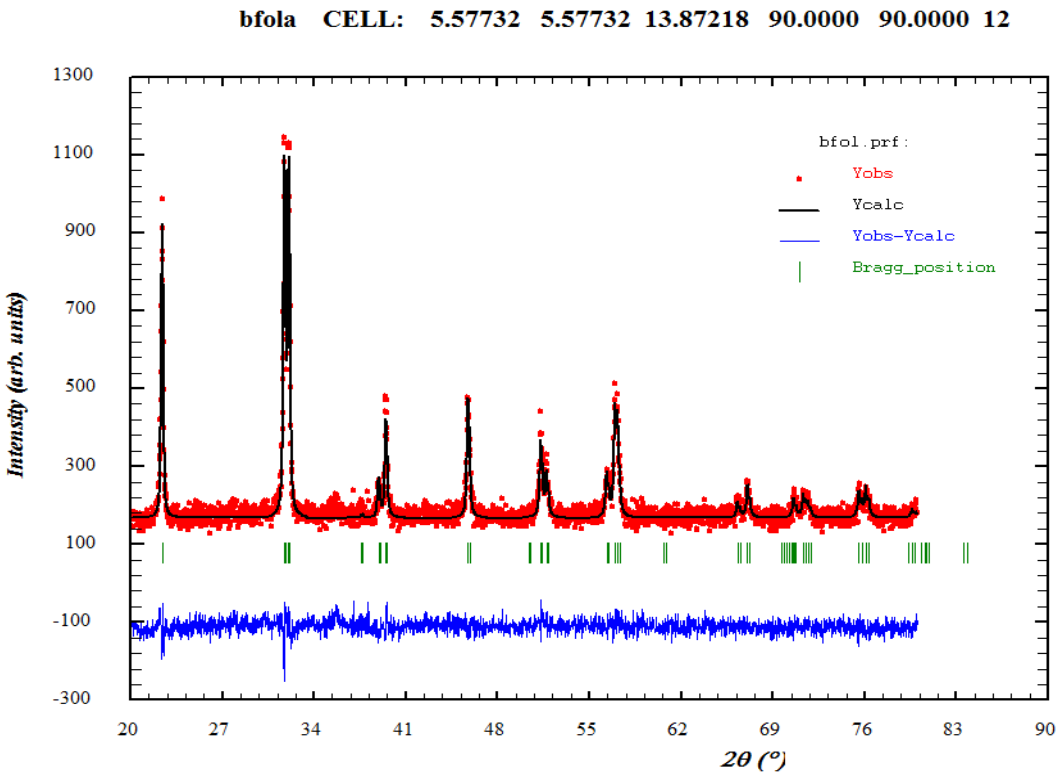

Figure 5(a). Rietveld refinement plot of BFO

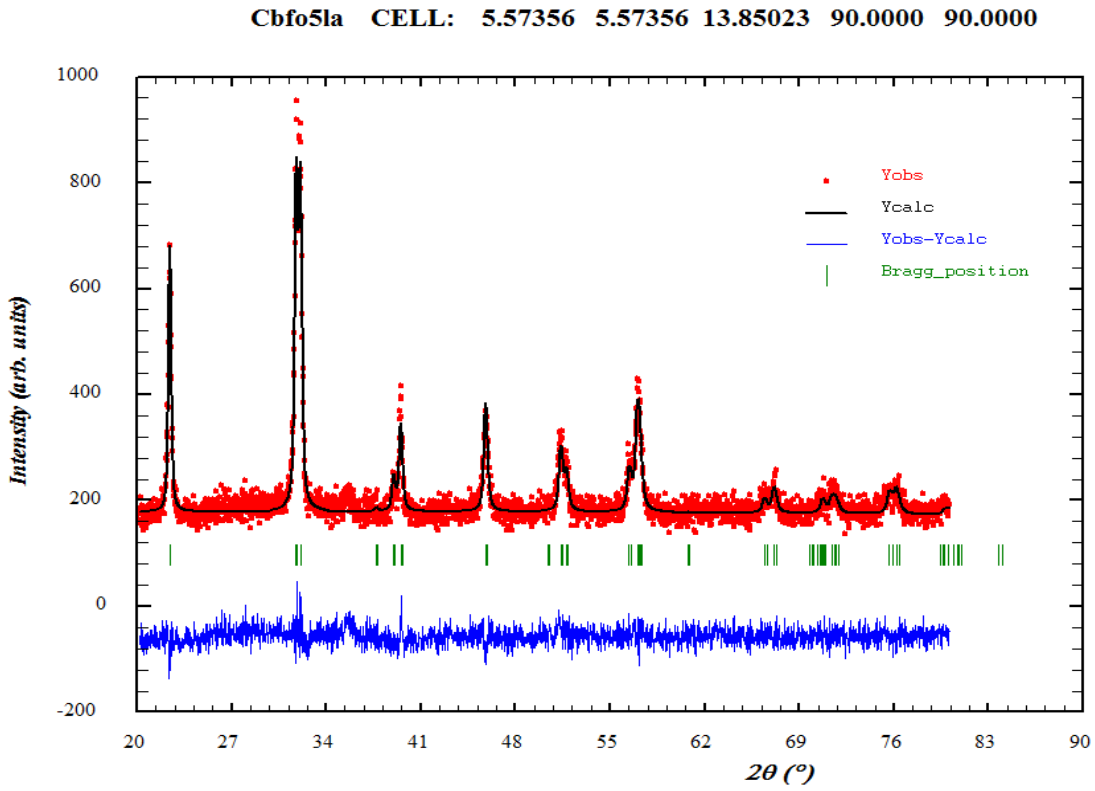

Figure 5(b). Rietveld refinement plot of CBFO5

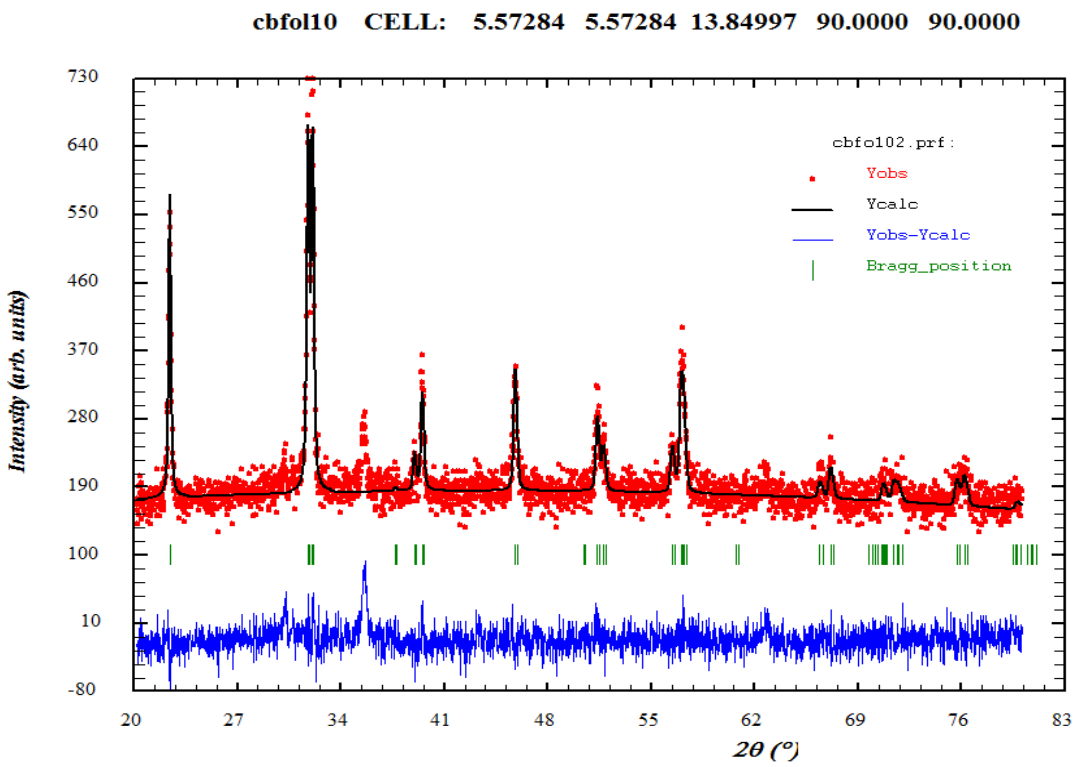

Figure 5(c). Rietveld refinement plot of CBFO10

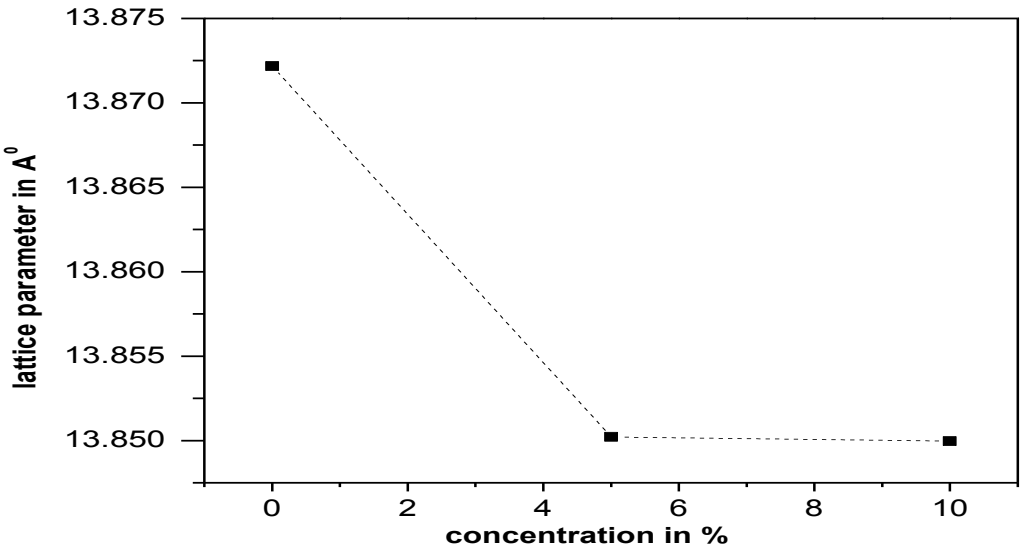

Figure 5(d). Decrease in lattice parameter (c) with concentration of cobalt

II. DSC and TG analysis:

The DSC and TG analysis of all the three samples is carried out using differential scanning calorimetric and thermo gravimetric analysis (DSC-TG) by heating the sample at 10 °C/min in argon in a thermal analyzer (Netzsch, Germany). The plots are shown in the figure 6(a), 6(b) & 6(c). Figure 6(a) shows the DSC and TG analysis of unleached & calcined BFO, by taking heat flow and mass loss in Y – axis and temperature in X – axis. In DSC, the heat flow increases with increase in temperature. The structure is unstable due to oxygen and bismuth loss around 820^0C to 870^0C above which an irreversible chemical decomposition of the sample occurs. Sharp endothermic peaks at 829^0C, 910^0C, 967^0C and 987^0C are observed. The peak at 830^0C corresponds to a reversible first order structural phase transition from R3c to P3mn, R3c being at lower temperature [8]. The peak at 910^0C shows bismuth loss phase as $Bi_2Fe_4O_9$. The strong peak at 967^0C corresponds to parasitic phase $Bi_2Fe_4O_9$ with Fe_2O_3 and large amount of liquid phase. The wider peak at 987°C corresponds to more liquid phase with Fe_2O_3 and disappearance of $Bi_2Fe_4O_9$. The TG plot of BFO reveals a broader decrease in mass near 100^0C due to evaporation of water molecules. As we gradually increase the temperature there is a considerable loss of mass around 300 - 400^0C, which is a broader one. It may be due to bismuth loss around this temperature, as bismuth is having boiling point of 275^0C.

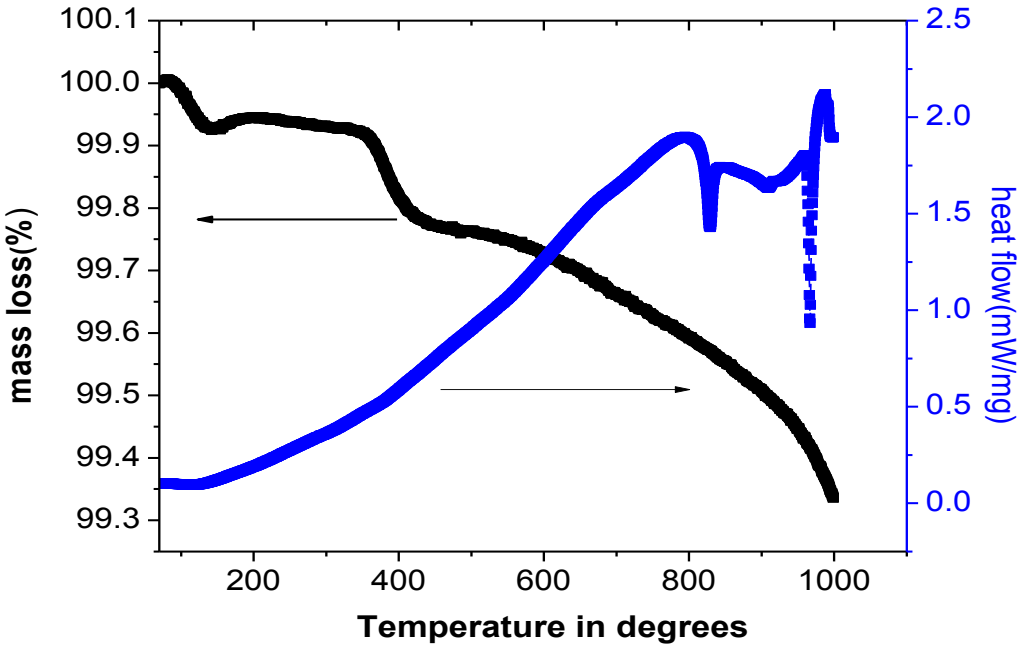

Figure 6(a). DSC and TG plot of unleached & calcined BFO

The DSC and TG plot of CBFO5 and CBFO10 samples are shown in the figure 6(b) and 6(c). The heat flow is continuously decreasing as we increase the temperature, which is yet to be understood. The mass is gradually decreasing and around 350^0C there is an increase in mass which may be due to formation of some new compounds by reaction of the sample with the atmosphere. The broader depression around 430^0C may be due to melting of the compound and presence of some liquid phase.

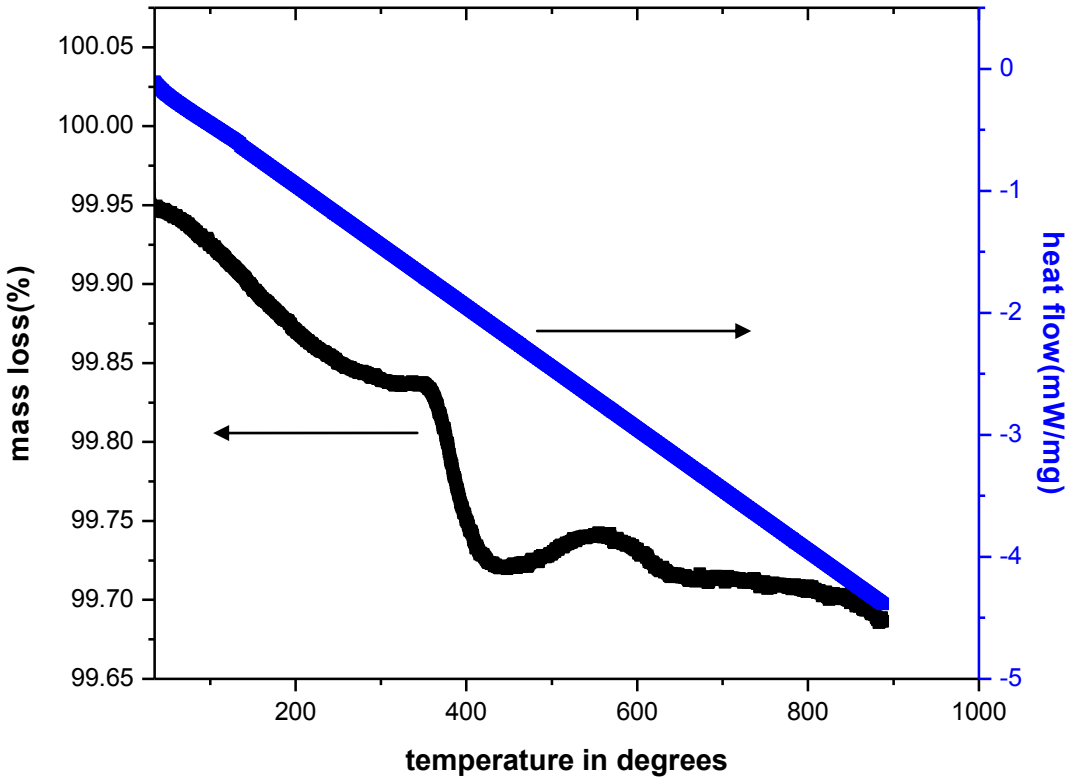

Figure 6(b). DSC and TG plot of unleached & calcined CBFO5

Similarly DSC and TG plot of CBFO10 represented in figure6(c). From the figure it is reflected that there is a greater absorbance of heat when we increase the temperature from the room temperature value. The broader endothermic peak around 280^0C shows there is a considerable amount of liquids are formed at this temperature. As we increase the temperature the heat flow is increased and around 800^0c there is exothermic peak corresponding to some new phase of the material. The mass loss plot shows there is a continuous decrease of mass as we increase the temperature and around 500^0C the mass loss rate is decreased and again it is saturated.

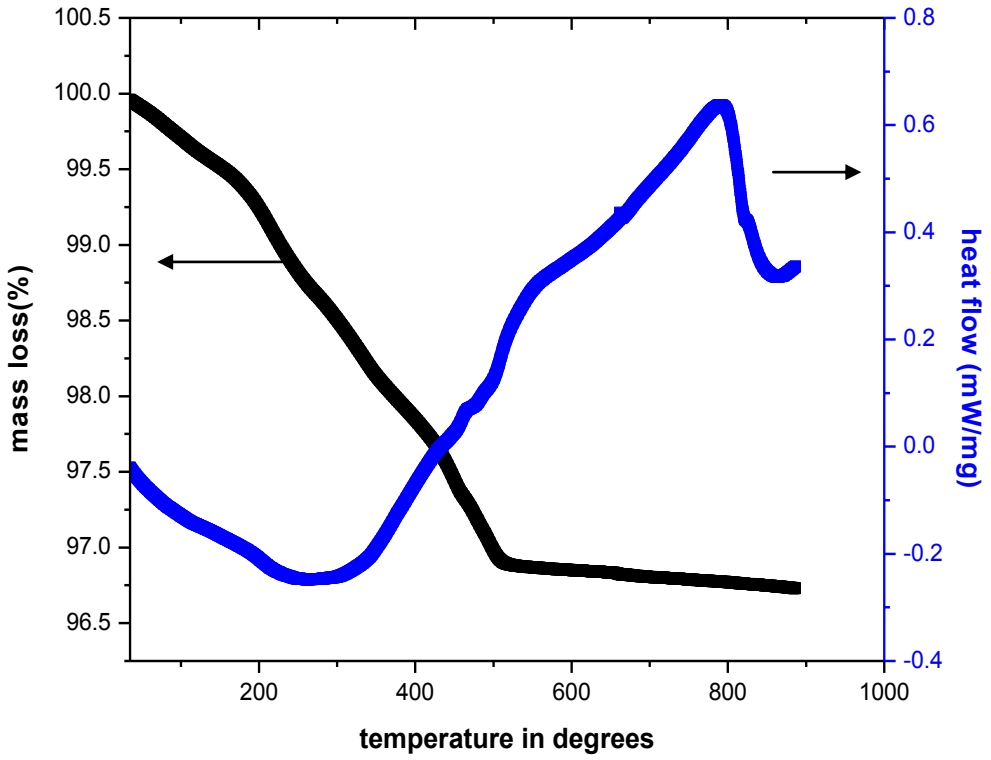

Figure 6(c). DSC and TG plot of unleached & calcined CBFO10

III. SEM Analysis:

Microstructural features were studied using Scanning Electron Microscope (JSM 6480 LV JEOL, Japan). The SEM microstructure of all samples is given in figure 7. All the samples are leached and sintered, except (a) which is unsintered. The sample (a) is in agglomerated form and it has no definite shape and size. Fig 7(b) & (c) shows the SEM of sintered samples at 700^0C. The microstructure of the samples sintered at 700^0c shows appearance of sharp features and blocks of various shapes and sizes (100 nm to 1μm). Another important thing one may observe while comparing the micrographs of the sintered samples that the grain size goes on decreasing as we increase the doping concentration of Cobalt. This result is well agreement with the x-ray diffraction data, which shows decrease in lattice volume with cobalt concentration. Due to some unavoidable circumstances the SEM image of CBFO10 sample cannot be done.

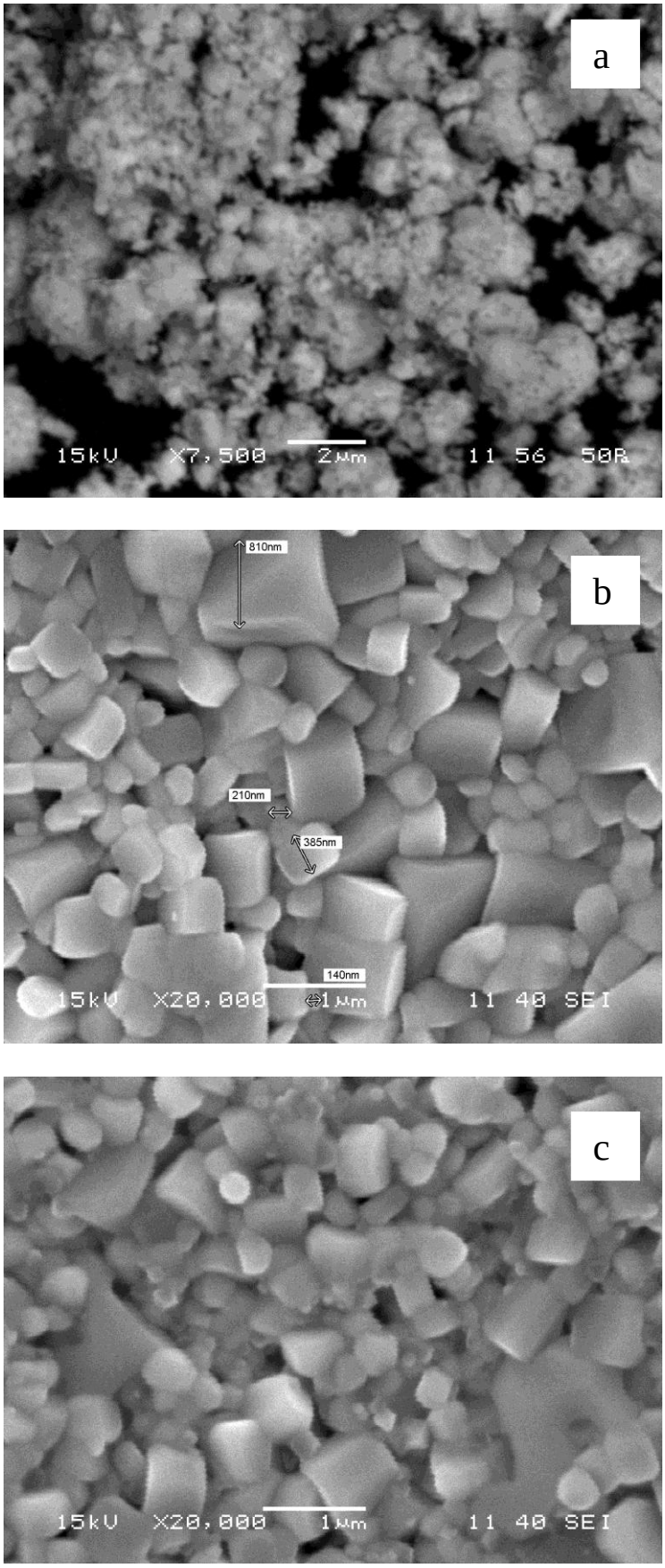

Figure 7. Surface morphology using SEM for (a) BFO powder (b) sintered BFO (c) CBFO5

IV. EDXS Analysis:

The Energy Dispersive X - ray Spectrometer (EDXS) analysis of all the three samples is shown in the following Figure 8 (a), (b) & (c). The EDXS plot reveals no extra peaks related to elements other than the constituents. All the samples show the exact match for standard peak position for Bi, Fe, Co and Oxygen. This reveals that the elemental composition of all the samples does not contain any foreign elements and if any parasitic phases are there, it has to be some form of Bi, Fe, Co, and oxygen only.

V. Dielectric properties analysis:

The dielectric measurement as a function of frequency in the range 100Hz to 1MHz, is done using HIOKI 3532 – 50 LCR Hi TESTER. Figure 9 shows the variation of dielectric constant with the frequency for BFO along with BFO doped with 5 & 10% of Cobalt. The low frequency dielectric constant for BFO is 36. There is a slight increase in the low frequency dielectric constant with Co – doping (54 and 202 for 5% & 10%Co doped BFO respectively). The dielectric constant for all the samples decreases continuously with increase in frequency; however the rate of decrease, increases with increasing Co-concentration. At high frequency, the dielectric data for BFO and CBFO5 reaches almost same value, where as that for CBFO10 is much-much lower than these two. At present it is difficult to exactly figure out the cause for such behaviour of these samples, as there may be various parameters responsible for this, such as charge defects, nonstoichiometry, secondary phases, etc [7]. Initial rise in the dielectric constant is favourable and definitely cobalt has some role in it. The large drop in the dielectric value of CBFO10 may be due to presence of secondary phases seen as peak at 35^0 in the x-ray diffraction plot, because this peak is seen only in 10% sample.

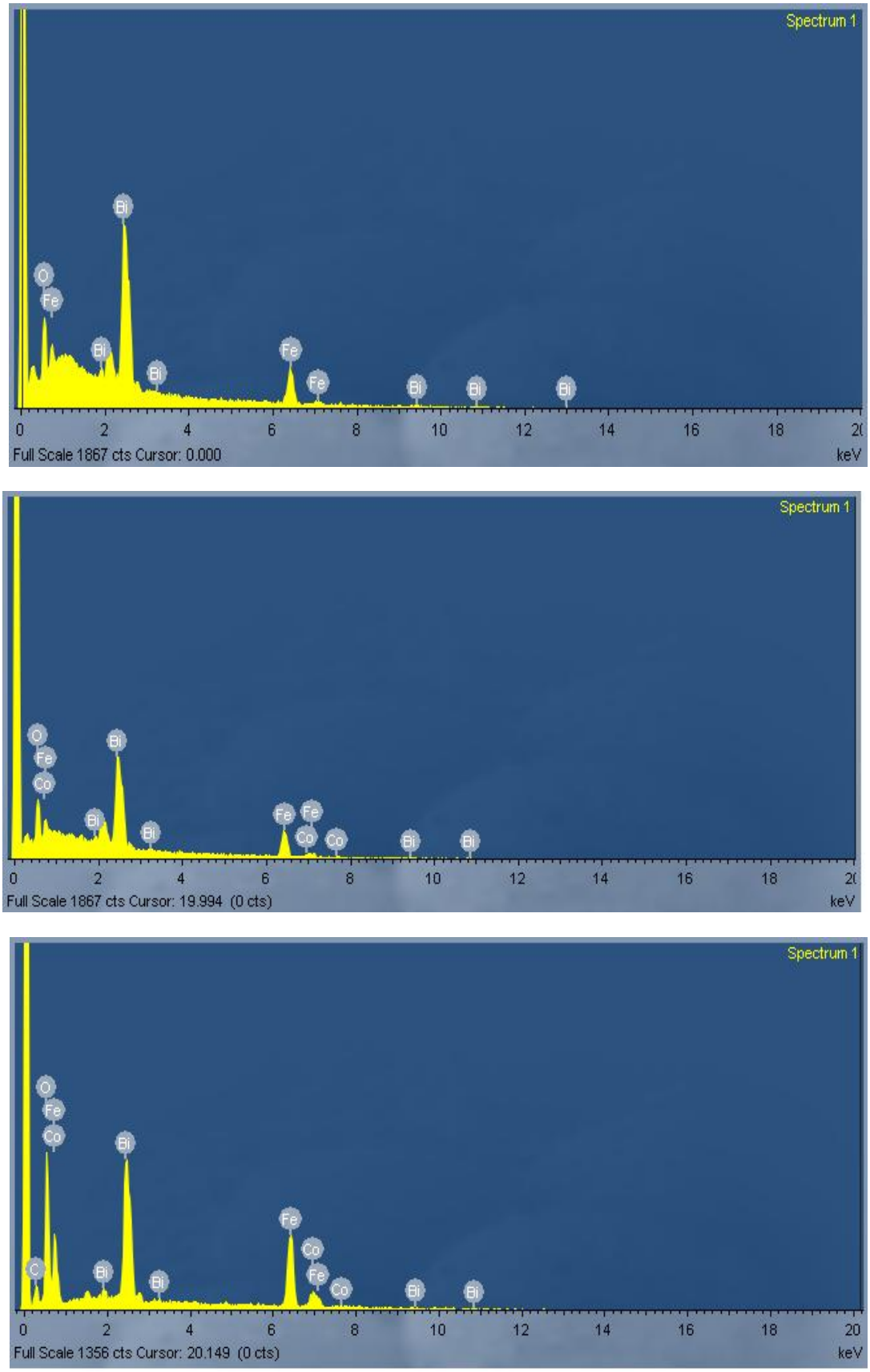

Figure 8. EDAX of (a) BFO (b) CBFO5 (c) CBFO10

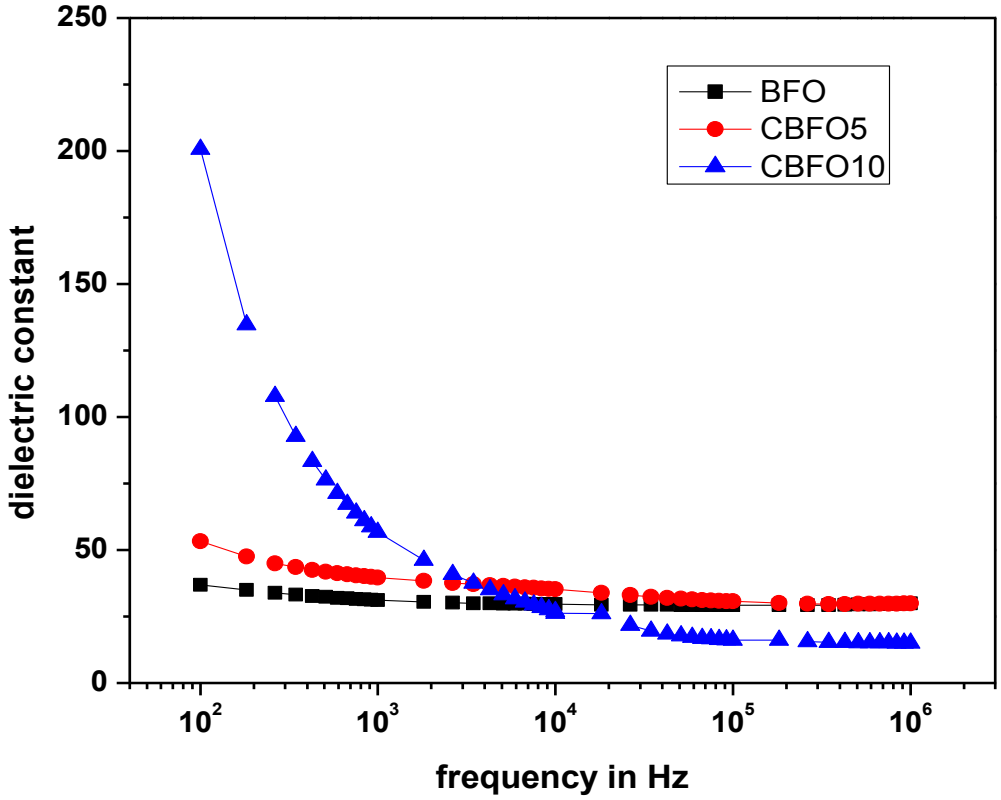

Figure 9. Variation of dielectric constant with frequency for BFO having 0%, 5% and 10% Co

CHAPTER 4: CONCLUSIONS

The sample is successfully prepared by liquid phase combustion synthesis method. Small amount of impurity phases are observed by x-ray diffraction results. The impurity phase grows with temperature and the sample calcined at 500 ^{0}C has less impurity phases than the sample calcined at 700 ^{0}C. From the literature survey, the impurity phases could be indexed to $Bi_2Fe_4O_9$ and $Bi_{25}FeO_{39}$. The cobalt doped BFO also found to be having impurity phases and it increases with increase in concentration of cobalt. However these impurity phases could be removed by leaching the samples in dilute nitric acid. Even after leaching, BFO with 10% cobalt, contain a foreign peak (as seen in xrd). The x-ray diffraction for all the samples are refined using Reitveld technique, in a freely available software FULPROF. Upon co-doping, the lattice volume of BFO decreases with cobalt concentration. This may be due to smaller ionic radius of cobalt (74 pm) than that of iron (78pm).

The Differential scanning calorimetry (DSC) and thermo-gravimetric (TGA) plot shows the behaviour of the sample with respect to temperature. From DSC plot it is observed that the heat flow increases with increase in temperature and structural transformation corresponding to R*3*c to P3mm is evidenced in the endothermic peak at 829 ^{0}C. Then few more successive endothermic peaks at 910^{0}C, 967^{0}C and 987^{0}C are observed. The broader peak at 910^{0}C corresponds to impurity phase $Bi_0Fe_4O_9$ and some iron loss phase Fe_2O_3. The sharp peak at 967^{0}C corresponds to less impurity phase $Bi_0Fe_4O_9$ and more iron loss phase Fe_2O_3 along with some liquid phases. The peak at 987^{0}C corresponds to total disappearance of impurity phases and presence of large amount of liquid along with some Fe_2O_3. The TG plot of BFO reveals a sudden decrease in mass near 100^{0}C due to evaporation of water molecules. As we gradually increase the temperature there is a considerable loss of mass around 300 - 400^{0}C, which is a broader one. It may be due to bismuth loss around this temperature, as bismuth is having boiling point of 275^{0}C.

From the SEM images of the BFO unsintered powder it is observed the powder is agglomerated and when this powder is sintered at 700 ^{0}C and made to pellet form, the SEM image reveals grains of tiny block with grain size varying from 100nm to 1μm. With increase in cobalt concentration there is shrinkage in grain size.

The EDXS plot reveals no extra peaks related to elements other than the constituents. All the samples show the exact match for standard peak position for Bi, Fe, Co and Oxygen. This reveals that the elemental composition of all the samples does not contain any foreign elements and if any parasitic phases are there, it has to be some form of Bi, Fe, Co, and oxygen only.

The dielectric constant plot with frequency shows that the low frequency dielectric constant for BFO is 36. There is a slight increase in the low frequency dielectric constant with Co – doping. The dielectric constant for all the samples decreases continuously with increase in frequency; however the rate of decrease, increases with increasing Co-concentration. At high frequency, the dielectric data for BFO and CBFO5 reaches almost same value, where as that for CBFO10 is much-much lower than these two.

REFERENCES:

1. H. Ibach and H. Luth, Solid-State Physics: An Introduction to Principles of Materials Science, 4th ed.(Springer Dordrecht Heildberg London New York,2009)

2. S. Somiya and F. Aldinger, Handbook of Advanced Ceramics: Processing and their applications, Vol-2. (Elsevier Academic Press,2009)

3. Scott *et al*.,"Multiferroic and magnetoelectric materials" Nature Reviews,**442**, 759(2009)

4. Lebeugle *et al.*,"Room temperature coexistence of large electric polarization and magnetic order in $BiFeO_3$ single crysatlal" ,Nature Reviews" Physical Review B.**76**, 024116 (2007)

5. Jian et al .," Progress and prospect for high temperature single-phased magnetic ferroelectrics", Chinese Science Bulletin. **53**, 2097(2008)

6. Lee *et al.*, "Single ferroelctric and chiral magnetic domain of single – crystalline $BiFeO_3$ in an electric field ", Physical Review B.**78**, 100101 (2008)

7. Zhao *et al.,* "Effects of Ion doping at different sites on electrical properties of multiferroic $BiFeO_3$ ceramics", J Applied physics D.**41**,065003(2008)

8. Haumont *et al.*,"Phase stability and structural temperature dependance in powdered multiferroic $BiFeO_3$", Physical Review B.**78**, 134108 (2008)

9. John A. Dean, Lange's handbook of Chemistry, 15th ed.(McGraw–Hill,New york)

10. Ramesh *et al*., "Electric modulation of conduction in multiferroic Ca-doped $BiFeO_3$ films" Nature materials", **8** , 485(2009)

11. Ramesh *et al*. "Electrical control of antiferromagnetic domains in multiferroic $BiFeO_3$ films at room temperature" Nature materials, **5** , 823(2006)

12. Ramesh *et al*., "Multiferroics: Progress and prospects in Thin Films"Nature Reviews",**6**, 21(2007)

13. Donna C. Arnold *et al.*, "Ferroelectric-Paraelectric Transition in $BiFeO_3$: Crystal Structure of the Orthorhombic β Phase",Physical Review Letters.**102**, 027602 (2009)

14. Kornev *et al.*," Finite-Temperature Properties of Multiferroic $BiFeO_3$" Physical Review Letters.**99**, 227602 (2007)

15. Cheng *et al.*, "Improved ferroelectric properties in multiferroic $BiFeO_3$ thin films through La and Nb codoping", Physical Review B.**77**, 092101 (2008)

16. Zhu *et al.*," Structural and magnetic characterization of multiferroic $(BiFeO_3)_{1-x}(PbTiO_3)$ solid solutions",Physical Review B.**78**, 014401 (2008)

17. Jiang *et al.*, "Synthesis and properties of multiferroic $BiFeO_3$ ceramics" J Electroceramics.**21**, 690 (2008)

18. Carvalo *et al.*, "Synthesis and thermodyanmic stability of multiferric $BiFeO_3$",Material Letters.**62**, 3984 (2008)

19. Hardy *et al.*, "Effects of precurssor chemistry and thermal treatment conditions on obtaining phase pure bismuth ferrite from aqueous gel precurssors",Journal of European Ceramic Society.**29**, 3007 (2009)

20. Xue *et al.*,"Low-temperature synthesis of $BiFeO_3$ nanoparticles by ethylenediaminetetraacetic acid complexing sol–gel process"Materials Research Bulletin.**43**, 3368 (2008)